AIP Advances

Microstructure evolution and the modification of the electron field emission properties of diamond films by gigaelectron volt Au-ion irradiation

Kuang-Yau Teng, Huang-Chin Chen, Chen-Yau Tang, Balakrishnan Sundaravel, Sankarakumar Amirthapandian, and I-Nan Lin

Citation: AIP Advances **1**, 042108 (2011); doi: 10.1063/1.3651462
View online: http://dx.doi.org/10.1063/1.3651462
View Table of Contents: http://scitation.aip.org/content/aip/journal/adva/1/4?ver=pdfcov
Published by the AIP Publishing

Microstructure evolution and the modification of the electron field emission properties of diamond films by gigaelectron volt Au-ion irradiation

Kuang-Yau Teng,[1] Huang-Chin Chen,[1] Chen-Yau Tang,[1] Balakrishnan Sundaravel,[2] Sankarakumar Amirthapandian,[2,3] and I-Nan Lin[1,a]

[1]*Department of Physics, Tamkang University, Tamsui, New-Taipei, Taiwan 251, Republic of China*

[2]*Materials Science Group, Indira Gandhi Centre for Atomic Research, Kalpakkam 603 102, India*

[3]*Institut für Halbleiteroptik und Funktionelle Grenzflächen, Universität Stuttgart, Allmandring 3, 70569 Stuttgart, Germany*

(Received 26 June 2011; accepted 12 September 2011; published online 4 October 2011)

The effect of 2.245 GeV Au-ion irradiation and post-annealing processes on the microstructure and electron field emission (EFE) properties of diamond films was investigated. For the microcrystalline diamond (MCD) films, Au-ion irradiation with a fluence of approximately 8.4×10^{13} ions/cm^2 almost completely suppressed the EFE properties of the films. Post-annealing the Au-ion irradiated MCD films at 1000°C for 1 h effectively restored these properties. In contrast, for ultra-nanocrystalline diamond (UNCD) films, the Au-ion irradiation induced a large improvement in the EFE properties, and the post-annealing process slightly degraded the EFE properties of the films. The resulting EFE behavior was still better than that of pristine UNCD films. TEM examination indicated that the difference in Au-ion irradiation/post-annealing effects on the EFE properties of the MCD and UNCD films is closely related to the different phase transformation process involved. This difference is dependent on the different granular structures of these films. The MCD films with large-grain microstructure contain very few grain boundaries of negligible thickness, whereas the UNCD films with ultra-small-grain granular structure contain abundant grain boundaries of considerable thickness. Au-ion irradiation disintegrated the large grains in the MCD films into small diamond clusters embedded in an amorphous carbon (a-C) matrix that suppressed the EFE properties of the MCD films. In contrast, the Au-ion irradiation insignificantly altered the crystallinity of the grains of the UNCD films but transformed the grain boundary phase into nano-graphite, enhancing the EFE properties. The post-annealing process recrystallized the residual a-C phase into nano-graphites for both films. [doi:10.1063/1.3651462]

I. INTRODUCTION

Diamond films have been investigated extensively for their application as electron field emitters because of their negative electron affinity and low effective work function.[1,2] While the physical properties of these films depend on the crystallinity of the materials, their electrical and optical characteristics are more closely related to the microstructure of the samples.[3] Ultra-nanocrystalline diamond (UNCD) film is a special form of diamond, which has recently attracted significant attention from researchers because of its unique granular structure.[4] While the grains of UNCD films have an sp^3 character, the grain-boundaries have a mixture of sp^2, sp^3, hydrocarbon and amorphous carbon,

[a]Author to whom correspondence should be addressed. Electronic mail: inanlin@mail.tku.edu.tw

in which the sp^2 character is predominant.[5] Because of the large field emission current density from UNCD as compared to other forms of diamond (nanocrystalline or microcrystalline), this material shows tremendous potential for applications such as cold cathode emitters and other vacuum microelectronic devices. The incorporation of nitrogen (N) into conventional microcrystalline diamond (MCD) with micron-sized grains can not effectively improve the conductivity and EFE properties of the films because N-species form deep donor levels and do not enhance the conductivity.[6,7] In contrast, the conductivity and EFE properties of UNCD films can be markedly improved by incorporating N into their grain boundaries.[4,6,7]

However, N incorporation via the addition of N_2 gas to the growth plasma is not efficient due to the small size of the UNCD grains. On the other hand, ion implantation (or irradiation) has long been used to modify the properties of materials through controlled doping with a variety of dopants.[8–10] Ion implantation (or irradiation) can break the C-C and hydrocarbon bonds to form sp^2 carbon. This effect can be used to tailor the sp^3/sp^2 ratio of diamond and related carbon materials by properly selecting the dose and energy of implantation.[9,10] The sp^2-bonded carbon in diamond films can be thought of as a conduction promoter, particularly if the sp^2 bonds form interconnected networks along which electrons are free to move. Control of the proportion of sp^2 bonds can be achieved by irradiation of the diamond thin films with energetic heavy ions. Much work has been carried out to improve the field emission of microcrystalline and nanocrystalline diamond by the ion implantation process.[10,11] Moreover, many reports have discussed the effects of ion beam irradiation on the characteristics of carbon based materials such as type IIa diamond,[12] diamond-like carbon films,[13] taC,[14] graphite[15] and polycrystalline CVD diamond films.[16–18] Furthermore, Pandey *et al.*[19] and Koinkar *et al.*[20] have studied the field emission enhancement by swift heavy ion irradiation in CVD diamonds; nevertheless, the mechanism for the modification of these characteristics remains unclear.

Here, we report the improvement effect of heavy-ion (2.245 GeV Au) irradiation on the electron field emission properties of microcrystalline diamond (MCD) and ultra-nanocrystalline diamond (UNCD) films. The modifications to the microstructure of these films due to heavy ion irradiation were investigated in detail using transmission electron microscopy (TEM), and the correlation of the granular structure evolution of these films with the resulting electron field emission (EFE) characteristics is discussed. Special attention is paid to the comparison of the difference in the Au-ion irradiation effects on MCD and UNCD films due to the different microstructures of these films.

II. EXPERIMENTAL PROCEDURES

The microcrystalline diamond (MCD) films were deposited using an H_2-plasma-based microwave plasma enhanced chemical vapor deposition (MPECVD) process, whereas the ultra-nanocrystalline diamond (UNCD) films were deposited using an Ar-plasma-based MPECVD process, for 60 min using an IPLAS reactor (Innovative Plasma Systems GmbH, CYRANNUS-I). Prior to the deposition of diamond films, the silicon substrates were ultrasonicated in methanol solution, containing nano-diamond powder (~5 nm) and titanium powder, for 45 minutes to create nucleation sites. In the growth of MCD films, a gas mixture of CH_4 and H_2 with flow rates of 1 and 99 sccm, respectively, was excited by 1500 W microwave (2.45 GHz). The total pressure in the chamber was maintained at 45 torr. The substrate temperature was estimated to be around 575°C during the growth of the MCD films. In contrast, in the growth of UNCD films, a gas mixture of CH_4 and Ar with flow rates of 1 and 99 sccm, respectively, was excited by 1200 W microwave radiation at 2.45 GHz, and the total pressure in the chamber was maintained at 100 torr. The substrate temperature was estimated to be around 475°C during the growth of the UNCD films.

The MCD and UNCD diamond films, around 300 nm in thickness, were subjected to 2.245 GeV Au-ion irradiation from the Universal linear accelerator (UNILAC) at GSI Helmholtzzentrum für Schwerionenforschung GmbH, Darmstadt, Germany, with fluences of 8.4×10^{13} ions/cm^2. The post-annealing process was conducted in a 5% H_2/Ar atmosphere at 1000°C for 1 hour. The 2.245 GeV gold ions have a projected range of 66.4 μm in diamond with longitudinal straggling

of 1.93 μm as simulated with SRIM-2008.[21] Therefore, the Au-ions will pass through the diamond films and get buried deep in the substrate for all the samples. There is no doping effect due to the Au-ion irradiation. The Au-ions have an electronic energy loss of 3.34×10^4 eV/nm and a nuclear energy loss of 28.99 eV/nm, which indicates that the ions will lose energy mostly through electronic excitations in the diamond. The lattice damage effects of nuclear energy loss will be minimal.

The films were characterized using scanning electron microscopy (SEM: Jeol JSM-6500F), Raman spectroscopy (Renishaw with excitation wavelength of 514.5 nm) and transmission electron microscopy (Jeol 2100). Electron field emission (EFE) properties of the diamond films were measured with a tunable parallel plate set-up in which the sample-to-anode distance was varied using a micrometer. The current density–electric field (J-E) characteristics were measured using an electrometer (Keithley 237) under pressures below 10^{-6} torr. The EFE parameters were extracted from the obtained J-E curves with the Fowler–Nordheim model[22] where the turn-on field was designated as the intersection of the lines extrapolated from the low field and high field segments of the Fowler-Nordheim plots.

III. RESULTS AND DISCUSSION

A. Effect of Au-ion irradiation on the MCD films

Figure 1 shows that the 2.245 GeV Au-ion irradiation ($8.4x10^{13}$ ions/cm^2) induced dramatic changes in the surface morphology of the microcrystalline diamond (MCD) films. The size of the grains was reduced from 500-900 nm for pristine MCD films (Fig. 1(a)) to around 300 nm for Au-ion irradiated films (Fig. 1(b)). The grains remained in a faceted geometry. Post-annealing the Au-ion irradiated MCD films did not further change their granular structure (not shown). Some aggregates of nano-sized grains (around 50-80 nm) occurred, distributed among the faceted grains (investigated in detail by TEM below). Raman spectroscopy, shown in Fig. 2(a), indicates that the pristine MCD films contain a sharp D-band resonance peak at 1332 cm^{-1}, the characteristic F_{2g} band for diamond lattices (curve I). Small broad resonance peaks near 1140 cm^{-1}, 1400 cm^{-1} and 1580 cm^{-1} were also present; these peaks are associated with disordered carbon.[23,24] However, because Raman spectroscopy is several times more sensitive to sp^2-bonds than it is to sp^3-bonds, the presence of an sp^2-related resonance peak in the Raman spectrum does not mean that the samples contain a large proportion of disordered carbon. Au-ion irradiation markedly decreased the intensity of the Raman resonance peaks (curve II), indicating that some proportion of the diamond phase was transformed into non-diamond phase material due to the Au-ion irradiation. Post-annealing of the Au-ion irradiated samples partially restored the Raman resonance peaks (curve III), implying that part of the transformed phase was re-crystallized into the diamond phase. The EFE behavior of the pristine MCD films can be turned on at $(E_0)_{pristine}$=29.2 V/μm, with an electron field emission current density of $(J_e)_{pristine}$=0.25 mA/cm^2 at an applied field of 80 V/μm (curve I, Fig. 2(b)). The Au-ion irradiation at a fluence of $8.4x10^{13}$ ions/cm^2 significantly suppressed the electron field emission (EFE) properties of the diamond films (curve II, Fig. 2(b)). The post-annealing process effectively restored the EFE properties of the films. The EFE turn-on field of the irradiated/post-annealed films was the same as E_0 for the pristine films ($(E_0)_{irrad/anneal.}$=33.2 V/μm). The post-annealed films achieved a large EFE current density of $(J_e)_{irrad/anneal.}$=0.3 mA/cm^2 at an applied field of 72.0 V/μm (curve III, Fig. 2(b)), which is markedly better than that of the pristine MCD films ($(J_e)_{pristine}$= 0.05 mA/cm^2 at 72.0 V/μm).

The change in morphology and Raman structure of the MCD films can not clearly account for the source of modification on the EFE behavior for these films due to Au-ion irradiation and post-annealing processes. To understand the factor that alters these characteristics, the detailed microstructure was examined using TEM. Figure 3(a) shows the typical granular structure of the pristine MCD films, where only the grains oriented near some zone-axis strongly diffract electrons and show high contrast. The adjacent grains are oriented away from the zone-axis, showing no contrast. The discrete spot patterns in the selected area electron diffraction patterns (SAED, inset in Fig. 3(a)) indicates that the MCD grains are near $01\bar{1}$ zone-axis, whereas the diffraction spots arranged along a ring, indicate that the background material contains other diamond grains that were

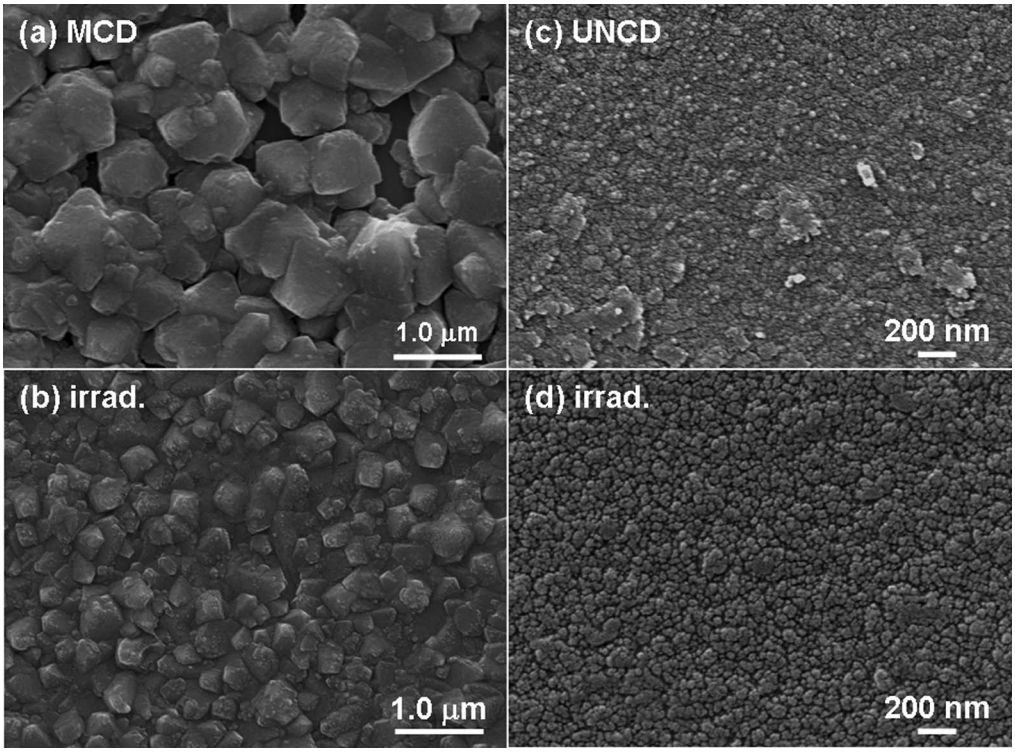

FIG. 1. SEM micrographs for the (a) pristine and (b) Au-ion irradiated (8.4 x 10^{14} ions/cm^2) microcrystalline diamond (MCD) films; those for the (c) pristine and (d) Au-ion irradiated (8.4 x 10^{14} ions/cm^2) ultrananocrystalline diamond (MCD) films.

randomly oriented. To more clearly illustrate the microstructural features of the MCD films, the dark field (DF) images taken from different diffraction spots from the SAED designated in Fig. 3(a) were superimposed. The composed DF image shown in Fig. 3(b) reveals that the region in adjacent to the grains A (pink color) is another diamond grain (B, green color), which is in different orientation. The boundaries between the grains A and B (designated as dotted squares, Fig. 3(b)) are sharp and clear, which will be detailed examined shortly.

The high resolution TEM micrograph shown in Fig. 4(a) reveals the structure image of central region of grain A in Fig. 3(a), indicating that the MCD grains contain complicated microstructure. The Fourier transformed diffractogram (F-T) of the whole structure image (FT_{0a}) indicates, again, that the pristine MCD is basically of cubic diamond structure (3C diamond) oriented in $01\bar{1}$ zone-axis. FT images of the designated areas indicate that, in addition to the defectless regions of 3C diamond with $01\bar{1}$ zone-axis (region 1 & FT_1), there are regions that contain stacking faults (regions 2), which are implied by the rel-rod associated with the major diffraction spots in FT_2 image, and regions of hexagonal symmetry, a polymorph of diamond (8H diamond, region 3),[23] which are implied by the systematic rows of diffraction spots in FT_3 image. Moreover, the TEM structure image of the region near the boundaries between the grains (designated as dotted square in Fig. 3(b)) is shown in Fig. 4(b), which reveals that the grain boundaries in the pristine MCD films are sharp and clear, i.e., no secondary phase was present in these grain boundaries.

Au-ion irradiation markedly alters the microstructure of the MCD films. Figure 5(a) shows that, in addition to the large diamond grains that survive the ion irradiation and still preserve good crystallinity, there are regions consisting of small clusters (region D). Figure 5(b) shows that, when the samples are tilted slightly away from the zone-axis such that the large grains are out of contrast, the small clusters are clearly observable. The SAED shown in inset of Fig. 5(b) implies that these small clusters are randomly oriented nano-diamond. Restated, the Au-ion irradiation generally has broken down the grains of the MCD films into about one-half to one-third of their original size

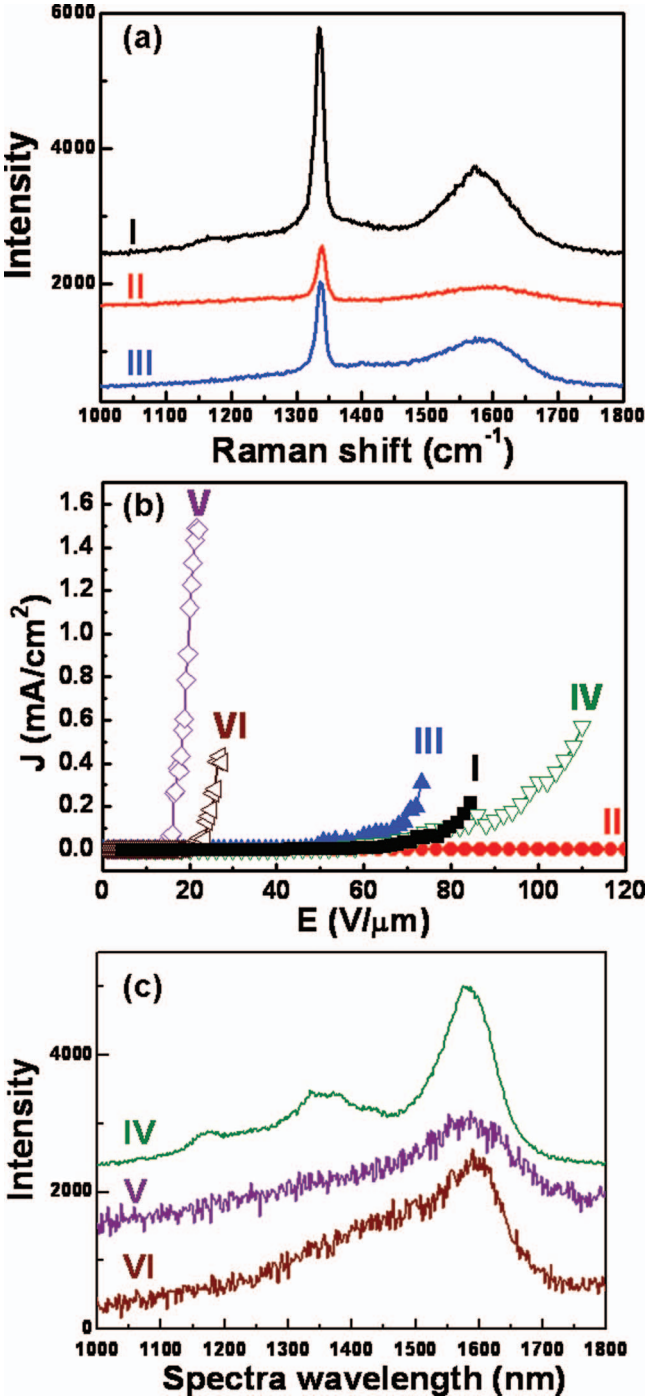

FIG. 2. (a, c) Raman spectroscopy of and the (b) the electron field emission properties for the MCD and UNCD films: (I) pristine, (II) Au-ion irradiated (8.4 x 10^{14} ions/cm^2) and (III) irradiated/post-annealed (1000°C, 1 h) microcrystalline diamond (MCD) and (IV) pristine, (V) Au-ion irradiated (8.4 x 10^{14} ions/cm^2) and (VI) irradiated/post-annealed ultrananocrystalline diamond (UNCD) films.

(cf. Figs. 1(a) and 1(b)), and, occasionally, has disintegrated the large diamond grains into small diamond particulates. To more clearly illustrate the phase constituents of these materials, a micrograph was composed, again, by superimposing the dark field images taken from the diffraction spots of the SAED (cf. Fig. 5(a)). Figure 5(c) indicates that, while the large grain (region C, yellow color) is 3C diamond oriented along $01\bar{1}$ zone-axis, which is implied by the spot-SAED shown in the inset of

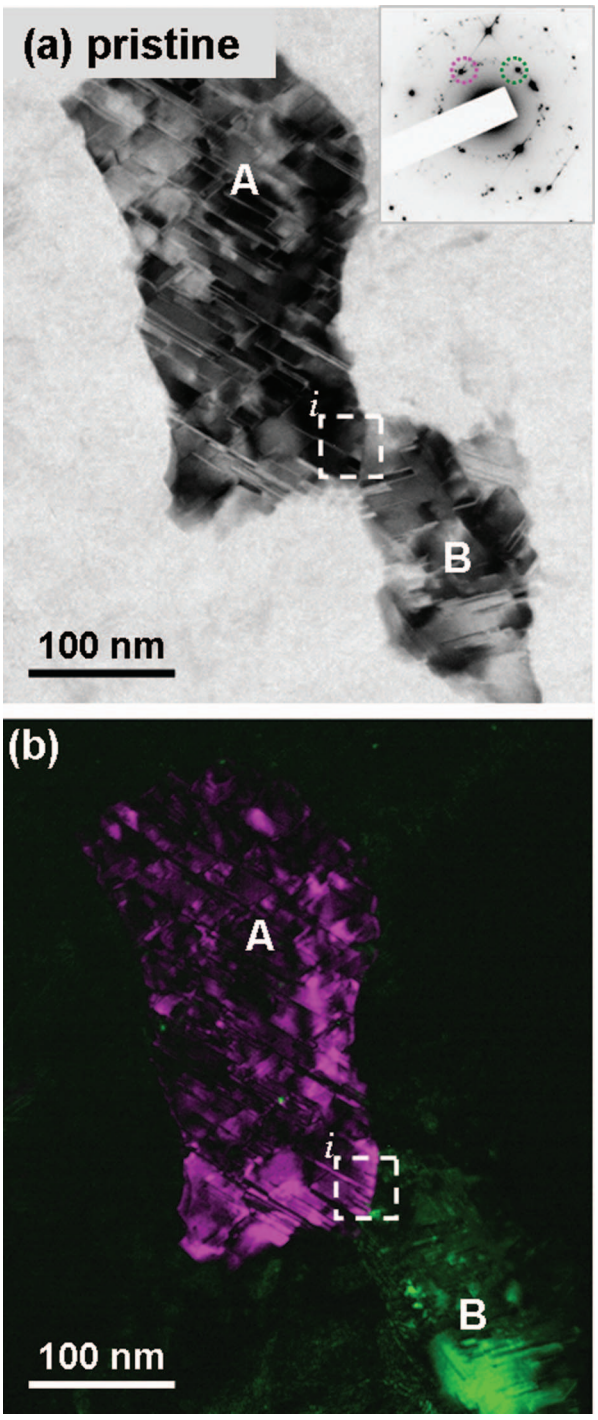

FIG. 3. (a) Bright field and (b) dark field low magnification TEM micrograph for the pristine MCD samples (the inset in (a) shows the corresponding selected electron diffraction pattern, SAED).

Fig. 5(c), the small clusters consisted of nano-sized diamond (pink color) embedded in an amorphous carbon (a-C, red color) and there also exist small number of *i-carbon* particulates, the bcc structured carbon (green color). The microstructure of the small cluster region will be examined further in detailed shortly.

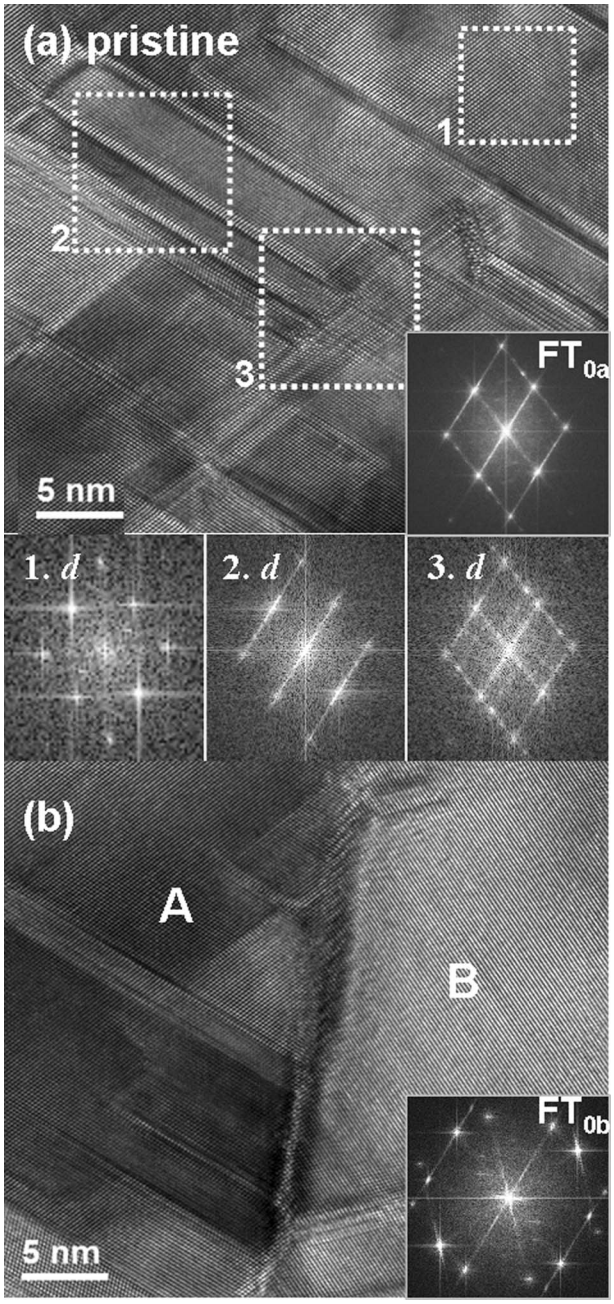

FIG. 4. TEM structure images for pristine MCD samples: (a) the central region of grain A and (b) the grain boundary region located in between grains A and B designated as dotted squares in Fig. 3(a) (the insets FT_{0a} and FT_{0b} are Fourier-transformed diffractogram corresponding to structure image in "a" and "b", respectively. The insets 1, 2 and 3 are FT images corresponding to areas 1, 2 and 3, respectively).

Enlarged TEM micrograph for region C of the as-irradiated MCD films (cf. Fig. 5(c)) is shown in Fig. 6(a), which is similar with the structure image of the pristine MCD grains (cf. Fig. 4(a)), except that the Au-ion irradiated MCD films are more heavily faulted and the parallel fringes are not as sharp as those in pristine films, indicating the existence of point defects in these faults. Such an observation implies that the Au-ion irradiation firstly induces the formation of point defects, the atomic vacancies or atomic displacements, which are then transformed into planar defects by *in-situ* recrystallization process. Figure 6(b) shows the enlarged TEM image of the interfacial region

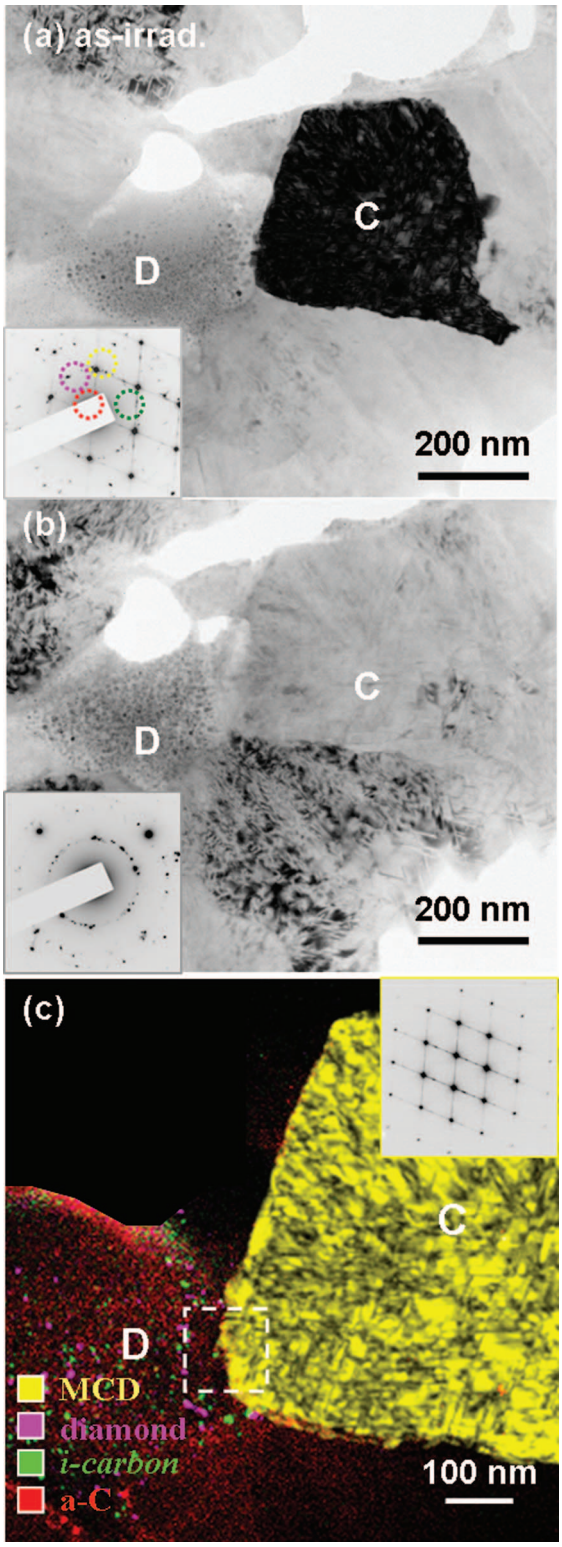

FIG. 5. (a, b) The bright field TEM micrograph of the as Au-ion irradiated MCD films with the region C of the samples aligned (a) or tilted away from (b) the $01\bar{1}$ zone axis (the insets show the corresponding selected electron diffraction pattern, SAED); (c) The composed dark field image, which is the superposition of the dark field images taken using the spots designated in inset of (a) of the as Au-ion irradiated MCD films.

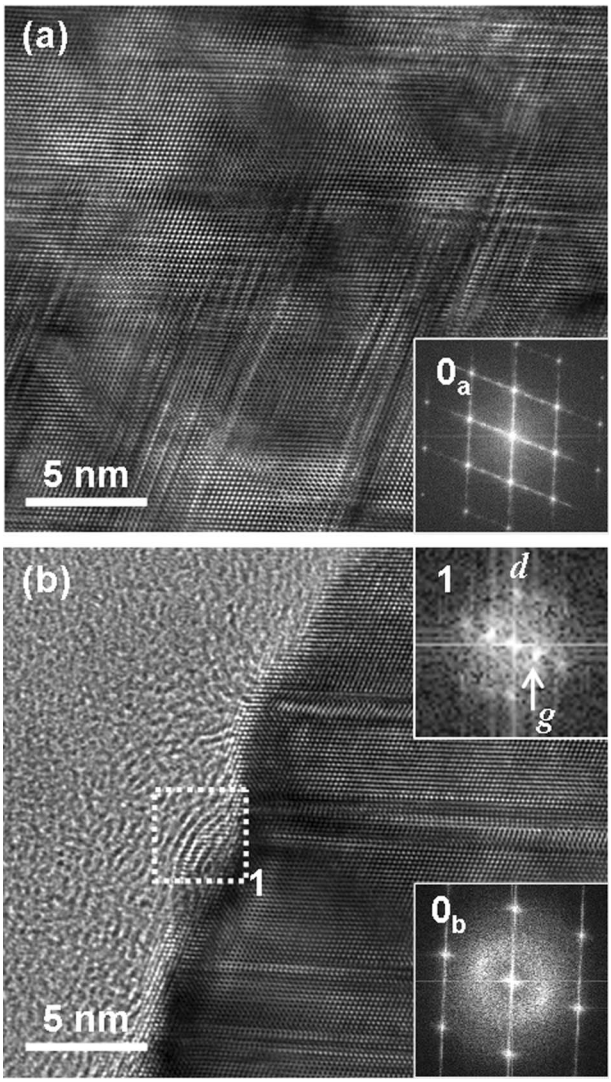

FIG. 6. The TEM structure image of as Au-ion irradiated MCD films: (a) the central region of diamond grains (region C in Fig. 5(c)) and (b) the interfacial region near large-grain and small-grain region designated as dotted square in Fig. 5(c). (The insets FT_{0a} and FT_{0b} are Fourier-transformed diffractogram corresponding to structure image in 'a" and "b", respectively. The inset FT_1 is the FT image corresponding to area 1.

located in between the large-grain and the small-cluster-areas (designated region, Fig. 5(c)). There is no clear boundary phase, except the presence of some nano-sized graphite phase (area 1, FT_1). The enlarged TEM micrograph for small-cluster area (region D, Fig. 5(c)) is shown in Fig. 7(a), which illustrates that the small cluster region contains spherical shaped clusters about 5-10 nm in size. The SAED (inset, Fig. 7(a)), in conjunction with the structure image shown in Fig. 7(b), indicates that these small clusters are basically randomly oriented nano-diamond particulates. Detailed analysis on the SAED in Fig. 7(a), using linear diffraction pattern (*ldp*) (Fig. 7(c)), indicates the presents small proportion of *i-carbon*, besides the nano-diamond particulates.. Moreover, large diffuse ring in the center of the SAED (inset, Fig. 7(a)) implies that the small-grain region contains large proportion amorphous phase. Restated, Au-ion irradiation disintegrated some of the large grains into small clusters, which mainly consist of nano-sized diamond embedded in a matrix of amorphous carbon. There also exists small proportion of *i-carbon*.

TEM examinations show that post-annealing of the Au-ion irradiated MCD films markedly alters the granular structure for the films. Figure 8(a) shows that the annealed MCD films also

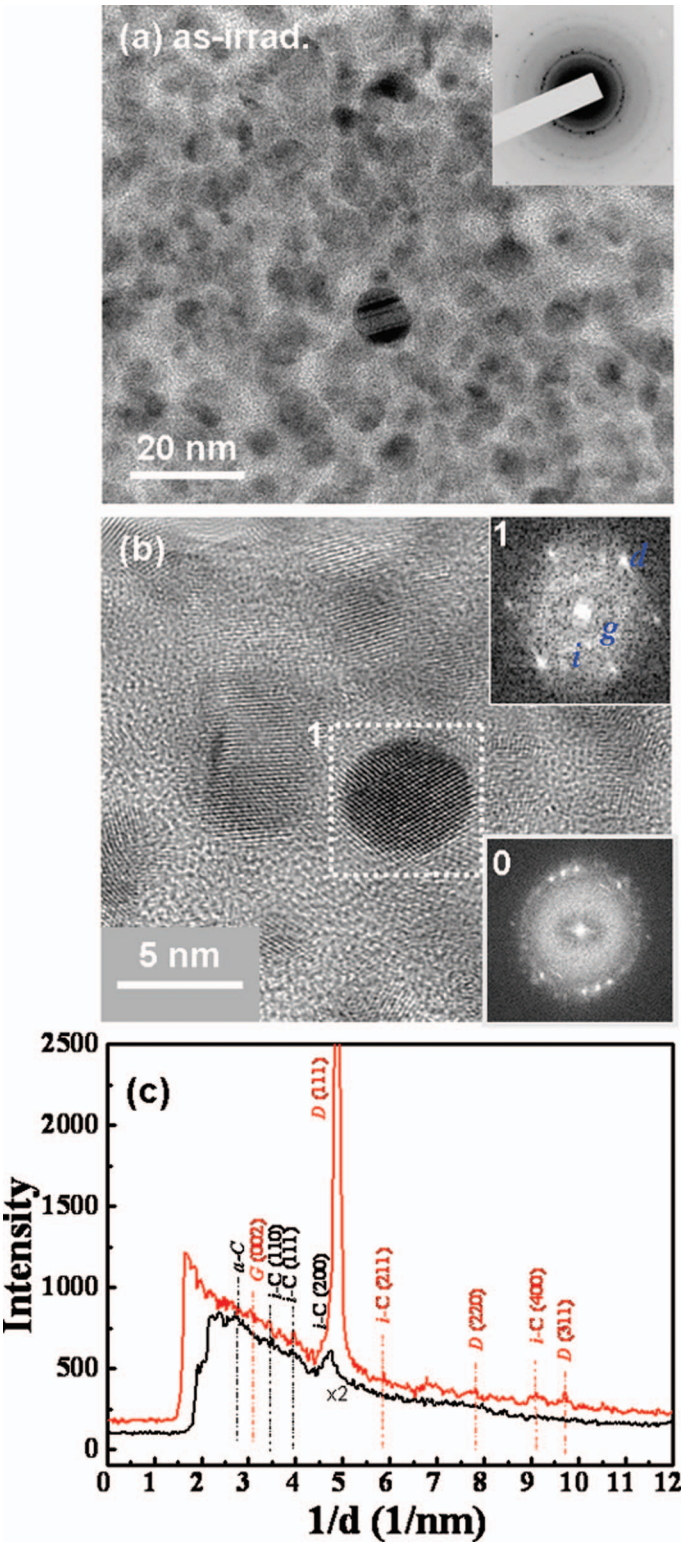

FIG. 7. The (a) high magnification TEM micrograph and (b) structure image of the small grain region (region D in Fig. 5(c)) with the inset in (a) showing the SAED. The insets in (b) show the Fourier-transformed diffractograms of the whole structure image in "b" (FT_0) and region 1 (FT_1), respectively; (c) the linear diffraction pattern derived from the SAED in "a".

contain a mixture of large-grain and small-grain regions, which are typically designated as regions E and F, respectively. The presence of small-grain region is more clearly illustrated by tilting the samples to render the large grain (region E) out of contrast (Fig. 8(b)). The structure image shown in Fig. 9(a) reveals that the large grains (region E) are also of well crystallized 3C diamond lying along $01\bar{1}$ zone-axis and contain stacking faults, which were indicated by the rel-rods associated with each diffraction spots in FT image (FT_{0a}, Fig. 9(a)). There also exists hexagonal diamond (area 1), which is implied by the systematic rows of diffraction spots in FT image (FT_1). The proportion of stacking faults in post-annealed MCD films is much less than that contained in the as-irradiated ones. These observations imply that the stacking faults are effectively healed, whereas the hexagonal diamond lattices will not be further transformed, by the post-annealing process.

Figure 9(b) shows the enlarged micrograph of the small grain region (region F, Fig. 8(a)), indicating that this region contains small grains with the size around 5-10 nm. The SAED shown as inset in Fig. 9(b) indicates that, in addition to the diffraction ring corresponding to 3C diamond phase, there exists some extra diffraction spots, which are arranged in a ring outside the (111) diffraction ring of diamond. These extra-spots correspond to *i-carbon*, the bcc structured carbon. One of the typical *i-carbon* particulate is illustrated in structure image shown in Fig. 9(c) (area 2, FT_2). The *ldp* patterns derived from the SAED (inset, Fig. 9(b)) is shown in Fig. 9(d), which reveals, again, that this region contain large proportion of *i-carbon*. The central diffused ring, which corresponds to amorphous carbon phase, is lower in intensity, as compared with those for the as-irradiated films (cf. Figs. 7(a) and 9(b)). Such an observation implies that the amorphous carbon surrounding the diamond clusters has been effectively re-crystallized into *i-carbon* due to post-annealing process. The distribution of the *i-carbon* particulates is more clearly illustrated in the composed dark field images in Fig. 8(c), which, again, is the superposition of the dark field images corresponding to different diffraction spots in the SAED (inset, Fig. 8(a)). The particulates of the diamond, i-carbon and nanographite in the Au-ion irradiated/post-annealed films are larger in size, as compared with those in the as-irradiated films (cf. Figs. 5(c) and 8(c)).

Moreover, Fig. 8(c) reveals that the re-crystallization of the small clusters into large-sized diamond crystals is also observed in the regions near the large grain (e.g. regions G_1, G_2 and H, Fig. 8(c)). It seems that the recrystallization process is somehow promoted near the original diamond grains (e. g. grain E). Detailed examination reveals the presence of a boundary phase between the original diamond grains (e.g. grain E) and the recrystallized ones. Figures 10(a) and 10(b) show two typical regions, which are the boundaries lying in between the grain G_1 and G_2 with the grain E, respectively (cf. Fig. 8(c)). These micrographs indicate the presence of an interfacial region with the thickness around 1-3 nm, which is markedly larger than the grain boundary region in pristine MCD films (cf. Fig. 4(b)). The phase in the interfacial region can be more clearly resolved when the large grain E was tilted away from the zone axis. Figure 10(c) illustrates the boundary lying in between grain H and E, revealing that the H-to-E interfacial region contains curved fringes (area 3, Fig. 10(c)). The corresponding FT image (FT_3) indicates that the spacing of the parallel fringes is around 0.34 nm, inferring that they are a-few-layer thick graphite. Presumably, the interfacial phases in Figs. 10(a) and 10(b) are also a-few-layer thick graphite, but are oriented in other direction and thus show no fringes. It should be noted that in the as-irradiated MCD films (cf. Fig. 6(b)), no such interfacial phase was observable, as the regions surrounding the large diamond grains are mostly the disintegrated nano-clusters region.

In the MCD films, electrons were mainly supplied from the underlying substrates, as there are no donors in the material. The transport behavior along the grain boundaries is thus the primary factor determining the EFE properties of the materials. In the pristine MCD films, the grain boundaries are sharp and clear, which results in poor electron transport properties, and a large turn-on field is required to trigger the EFE process. Au-ion irradiation significantly damages the diamond materials; even some of the large grains were disintegrated into small clusters. The small clusters of nano-sized diamond were dispersed in a matrix of amorphous carbon, which is highly resistive. Therefore, most of the electron conducting paths were blocked, and the EFE of the materials was significantly degraded due to the Au-ion irradiation process. The post-annealing process recrystallized the amorphous carbon into nano-sized crystals, which included nano-diamond, *i-carbon* and nano-graphite. The recrystallization process, which formed large diamond grains, also induced the formation of

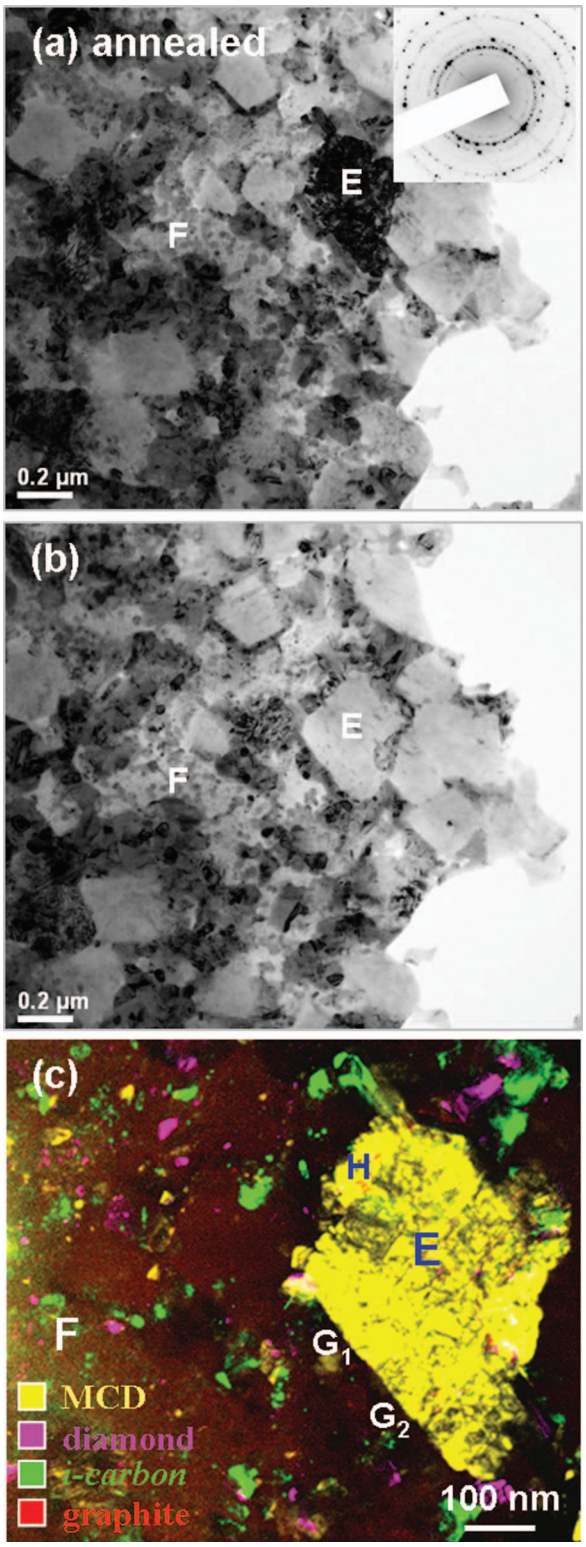

FIG. 8. (a, b) The low magnification TEM micrographs of Au-ion irradiated/annealed MCD films with the region E aligned (a) and tilted away (b) from a zone axis (the inset in "a" shows the SAED); (c) the composed dark field image, which is the superposition of the dark field images corresponding to different spots of SAED, showing the co-existence of large-diamond-grain with small-particulates regions. The latter consists of nano-sized diamond, *i-carbon* and nano-graphite.

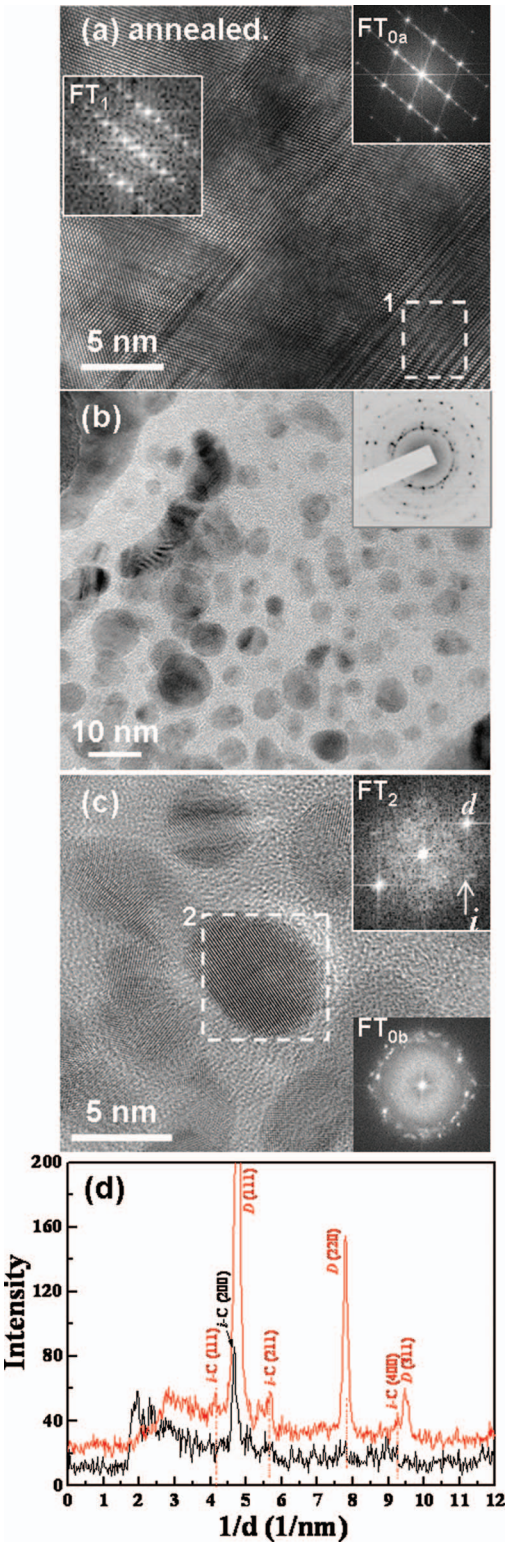

FIG. 9. (a) TEM structure image of the central region of grain E designated in Fig. 8(c); (b) the enlarged TEM bright field image and (c) the structure image of the small-grain region (region F in Fig. 8(c)), (d) the linear diffraction pattern derived from the SAED in "b".

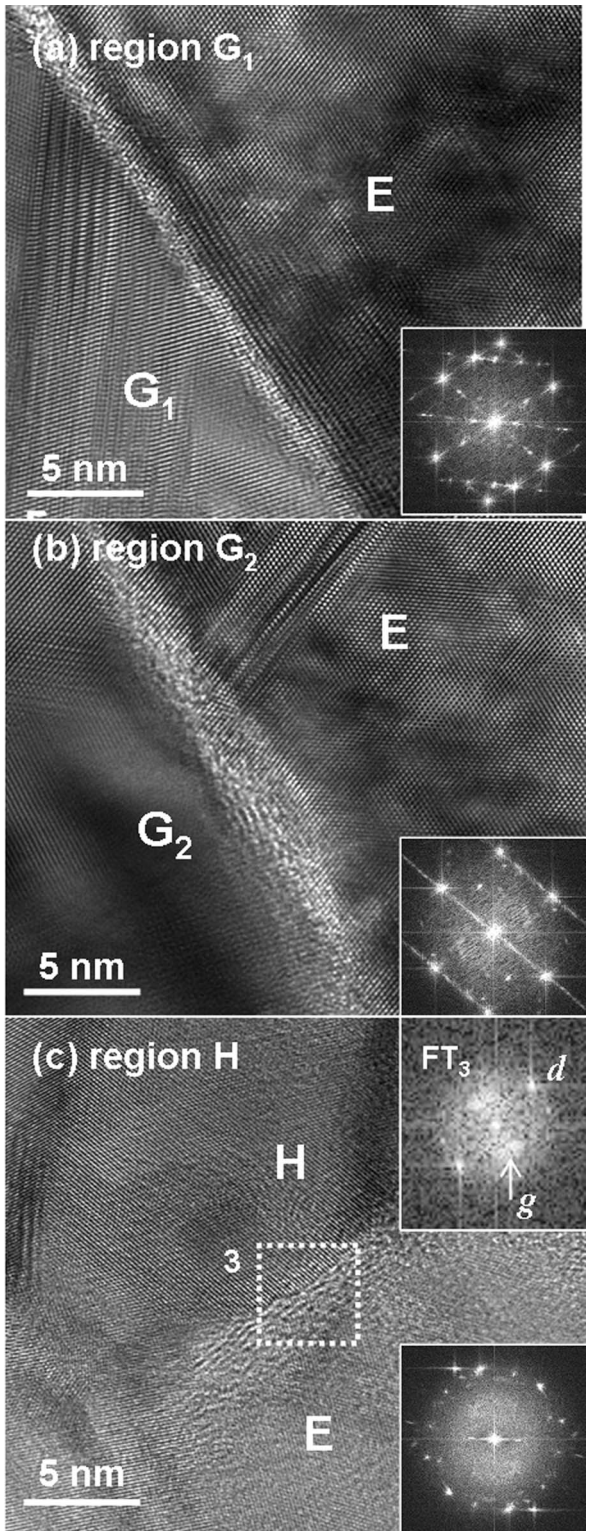

FIG. 10. (a) and (b) are the TEM structure images of the G_1-E and G_2-E interfacial regions designated in Fig. 8(c), respectively, and (c) those of the H-E interfacial region designated in Fig. 8(c), showing the presence of graphitic phase along the interfaces.

nano-crystalline graphite at the interfacial boundaries between the recrystallized diamond and the original diamond grains. The presence of nano-graphite markedly improved the electron transport, enhancing the EFE properties of the irradiated/annealed MCD films, which were even better than those of the pristine MCD films.

B. Effect of Au-ion irradiation on the UNCD films

Contrary to the common understanding that diamond is a very strong material that is not damaged by heavy ion irradiation, the above observations indicate that the granular structure of MCD films can be significantly modified if the Au ions have high energy and large fluence. The Au-ion irradiation induced the formation of planar defects, stacking faults, and even disintegration of large grains into nano-sized clusters when the fluence of Au ions exceeded a certain limit. The grain boundary regions are even more susceptible to damage from the heavy ion bombardment. The structural modification of the phases located adjacent to the grain boundary region is presumed to be the prime factor that influences the EFE behavior of the MCD films. On the other hand, the UNCD films consist of abundant grain boundaries due to the small grain size (~5 nm). These grain boundaries are of considerable thickness and contain hydrocarbon materials, which are more susceptible to the ion irradiation damage. It is expected that heavy ion irradiation will impose even more significant modification on the granular structure and EFE properties of the UNCD films, which is systematically investigated below.

The general effects of Au-ion irradiation on the characteristics of the UNCD films are shown together with those of MCD films in Figs. 1 and 2, to facilitate the comparison. While the SEM morphology of the UNCD films was barely altered by Au-ion irradiation (Figs. 1(c) and 1(d)), the Raman spectroscopy of these films were markedly modified. The Raman spectrum of the pristine UNCD films (curves IV, Fig. 2(c)) contains ν_1-band (1140 cm^{-1}) and ν_2-band (1480 cm^{-1}) resonance peaks, which correspond to trans-polyacetylene at the grain boundaries,[24,25] and D*-band (1350 cm^{-1}) and G-band (1580 cm^{-1}) resonance peaks, which correspond to disordered carbon.[26,27] These Raman spectra are characteristic of UNCD films with ultra-small grains. The D-band (1320 cm^{-1}) resonance peaks, which correspond to the F_{2g} resonance mode of the 3C diamond lattice, are only barely visible. The Raman spectra are markedly altered by the Au-ion irradiation. Curve V (Fig. 2(c)) shows that all the resonance peaks corresponding to UNCD materials are diminished, replaced by a noisy signal with a broadened peak near G*=1580 cm^{-1}, characteristic of the nano-graphite. This result implies that a large proportion of sp^2-bonds were induced. The significance of such a phenomenon will be further discussed shortly. Again, because visible Raman spectroscopy is more sensitive to sp^2-bonds than to sp^3-bonds, an sp^2 signal overwhelmingly larger than the sp^3 signal does not indicate that all the sp^3-bonded materials have been converted into sp^2-bonded materials. The Raman spectra were only moderately altered by the post-annealing process, i.e., the Raman signal was still noisy, and contained only the G-band resonance peak at 1580 cm^{-1}, which was slightly narrower (curve VI, Fig. 2(c)). Post-annealing of the Au-ion irradiated films at 1000°C (1 h) insignificantly modified the SEM morphology of the samples (not shown). Figure 2(b) (curves IV and V) shows that the Au-ion irradiation process markedly enhanced the EFE properties of the UNCD films. Specifically, this process lowered the turn-on field for the EFE process from E_0=30.0 V/μm to 11.6 V/μm and increased the EFE current density from J_e= <0.005 mA/cm^2 to 1.6 mA/cm^2 (at an applied field of 20 V/μm). The post–annealing process slightly degraded the EFE properties. Curve VI in Fig. 2(b) shows that the turn-on field was increased to $(E_0)_{an}$=13.5 V/μm, and the EFE current density was lowered to $(J_e)_{an}$= ~0.01 mA/cm^2 (at an applied field of 20 V/μm). However, these EFE properties are still better than those of the pristine UNCD films (curve IV, Fig. 2(b)).

Again, TEM microstructural investigation is needed for the purpose of understanding the genuine factor that influences the EFE behavior of the UNCD films due to Au-ion irradiation and post-annealing processes. Figures 11(a) and 11(b) show, respectively, the low magnification TEM micrographs for the pristine and as Au-ion irradiated UNCD films, whereas Figs. 11(c) and 11(d) show two typical regions of the Au-ion irradiated/ post-annealed UNCD films. These microstructures are very similar with one another. However, detailed analysis using dark field technique reveals the tremendous difference in the granular structure of the three films. The composed DF images shown

in Fig. 12 illustrate more clearly the phase constituents contained in each samples. It should be noted that each of the micrographs shown in Fig. 12 is the superposition of the dark field images corresponding to diamond, graphite and *i-carbon*. Firstly, the pristine UNCD films contain very few large diamond aggregates and small amount of amorphous phase (Fig. 12(a)). In contrast, the as Au-ion irradiated films contain abundant large diamond aggregates (Fig. 12(b)). TEM micrograph shown in Fig. 13(a) indicates the structure image of a typical aggregate in the Au-ion irradiated films. The aggregate seems to consist of small diamond clusters (~5 nm), which is twice as large as the size of the grains in the pristine UNCD films. Interestingly, all the smaller clusters, although seem to be separated by the faint boundaries, are aligned in the same orientation, implying that the coarsening process has occurred inside this aggregate. The diamond cluster in this aggregate will not be separated due to electron irradiation during TEM examination, i. e., the aggregate is an hard agglomerate. In contrast, the aggregates in the pristine UNCD films are soft agglomerates, as they were separated easily due to electron irradiation during TEM examination (not shown). There presents large amount of nano-graphite in the as Au-ion irradiated sample, which is implied by the FT image (inset in Fig. 13(a)). Post-annealing the Au-ion irradiated films insignificantly alters the population of large diamond aggregates (Fig. 12(c)). However, the TEM structure image of a typical aggregate in the Au-ion irradiated/post-annealed UNCD films (Fig. 13(b)), indicates that the faint boundaries between the diamond clusters were no longer exist, implying that the smaller diamond clusters have coalescence into a single large diamond grain due to the post-annealing process.

Moreover, besides the coalescence of diamond clusters into large diamond grains and the healing of the planar defects inside them, there are regions where rigorous phase transformation process has occurred. Low magnification TEM micrograph illustrated in Fig. 11(d) shows a region of the Au-ion irradiated/post-annealed films, which possesses the similar granular structure with that in Fig. 11(c). The diffraction ring in the SAED (inset, Fig. 11(d)) is actually larger than the typical (111) diamond ring. Such a larger diffraction ring corresponds to *i-carbon*, the bcc structured carbon. The composed dark field image of this region (Fig. 12(d)) reveals that these *i-carbon* particulates are as large as the coarsened diamond aggregates. The population of these *i-carbon* particulates is about the same as that of the diamond aggregates. Notably, the nanographite is always present along with the formation of *i-carbon* (cf. Fig. 12(d)). The phase constituents contained in the UNCD films is more clearly illustrated by the linear diffraction patterns (*ldp*), which are derived from the corresponding SAED shown as insets in Fig. 11. The *ldp* of these films are shown in Fig. 14, revealing that, while the pristine and as Au-ion irradiated films contain mainly the diamond (curves I & II, Fig. 14), the post-annealed films contain the graphite phase (e.g. Fig. 11(c) and curve III, Fig. 14) and the *i-carbon* (e.g. Fig. 11(d) and curve IV, Fig. 14). Notably, Figs. 11(c) and 11(d) are different regions of the same samples, indicating that the phase transformation process has proceeded differently in different regions.

Figures 15(a) and 15(b) show structure image of typical diamond and i-carbon particulates, respectively. The enlarged structure images of the designated areas are shown in Figs. 15(c) and 15(d), respectively, to indicate that, while both particulates have very similar structure (oriented in $01\bar{1}$ zone axis), the lattice spacing in Fig. 15(c) is 2.06 angstrom, which correspond to (111) interplanar spacing of diamond (d_{111}), while that in Fig. 15(d) is 2.54 angstrom, which corresponds to interplanar spacing of *i-carbon* (d_{111}). These micrographs confirm the presence of *i-carbon* particulates in the Au-ion irradiated/post-annealed UNCD films. Presumably, *i-carbon* particulates were transformed from the amorphous carbon during post-annealing process. These results imply that the Au-ion irradiation process altered the granular structure of the UNCD films in a non-uniform manner. In some regions, the diamond grains are only moderately damaged and the post-annealing process has induced the grain growth process, whereas, in other regions, the diamond grains are seriously damaged such that the post-annealing process has triggered the phase transformation toward more stable phase, the sp^2-bonded graphite. The *i-carbon* is an intermediated phase formed in accompanied with the formation of nano-graphite.

The above-described phenomena indicate that the Au-ion irradiation and post-annealing processes modify the granular structure of the UNCD films in a different way from that of the microstructure of the MCD films. The difference in the ion irradiation effect on the modification of the granular structure and the EFE properties of the MCD and UNCD films is probably due to the different

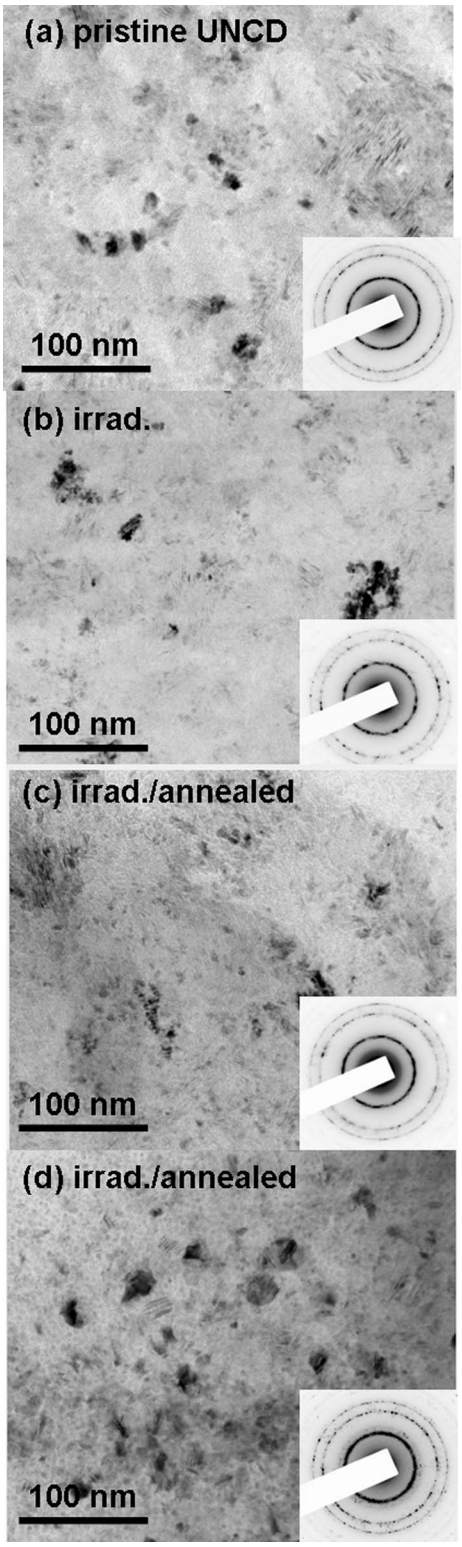

FIG. 11. The low magnification TEM micrographs of UNCD films: (a) pristine, (b) Au-ion irradiated and (c, d) irradiated/post-annealed.

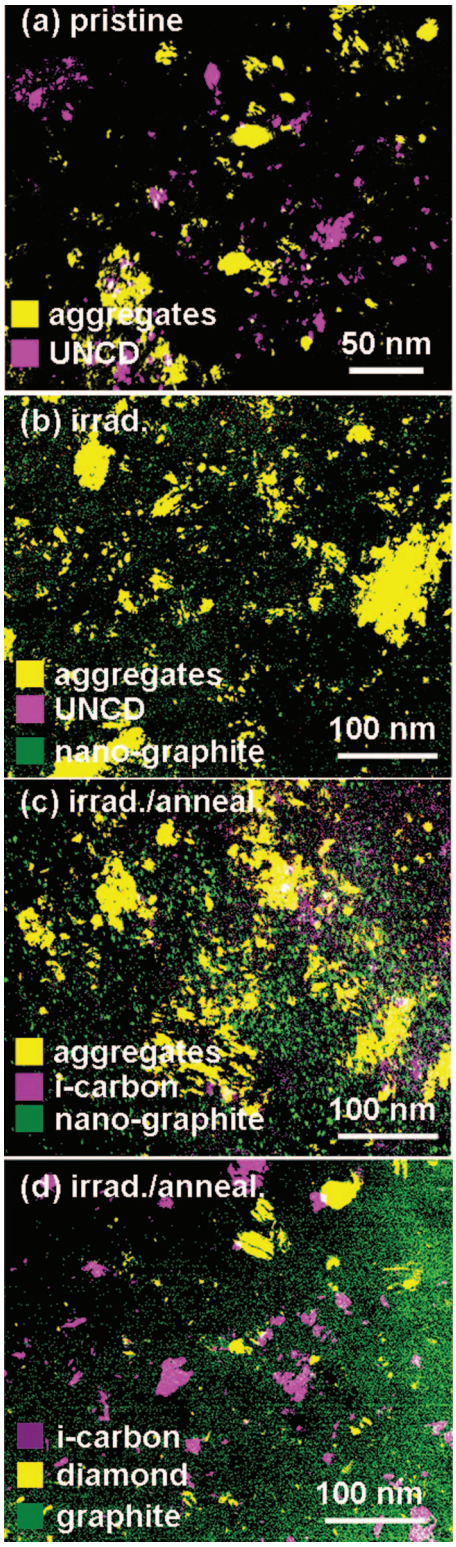

FIG. 12. The composed TEM dark field images of UNCD films corresponding to diamond, nano-graphite and *i-carbon*: (a) pristine, (b) Au-ion irradiated and (c, d) irradiated/post-annealed.

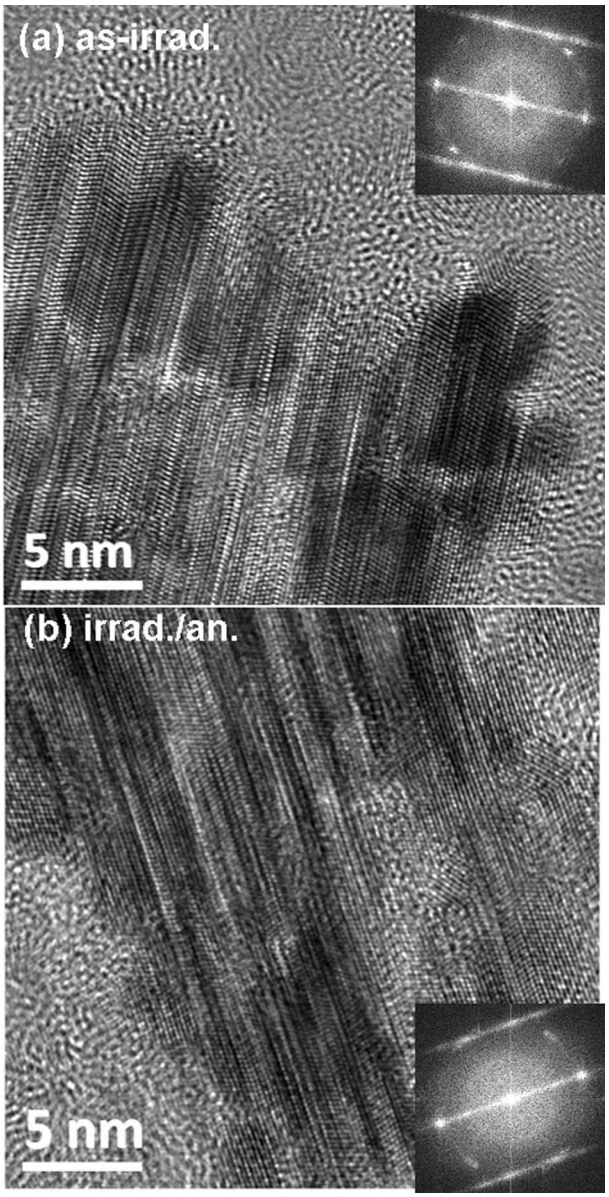

FIG. 13. The TEM structure image of a typical large aggregate in (a) as Au-ion irradiated and (b) Au-ion irradiated/post-annealed UNCD films.

microstructures of the two films. The grain boundaries of the MCD films are sharp and contain no amorphous carbon. Au ions can only impose irradiation damage on the diamond lattices, which requires large dissociation energy. The kinetic energy of the Au ions is only sufficient to disintegrate the diamond grains into smaller diamond grains (or to nano-sized clusters) with the amorphous carbon as a byproduct, but it is not able to induce the simultaneous recrystallization of the amorphous carbon surrounding the disintegrated particulates. The post-annealing process is required to repair the atomic defects in the diamond grains and convert the amorphous carbon located between the diamond grains into nano-graphite (or *i-carbon*). In contrast, the UNCD films contain nano-sized diamond grains with abundant grain boundaries of considerable thickness. The nano-sized grains are not further disintegrated by absorption of the kinetic energy of the incident Au ions. Most of the kinetic energy of the Au ions acted to dissociate the hydrocarbons in the grain boundaries and, furthermore, produced large transient thermal spikes that induced *in situ* re-crystallization of the

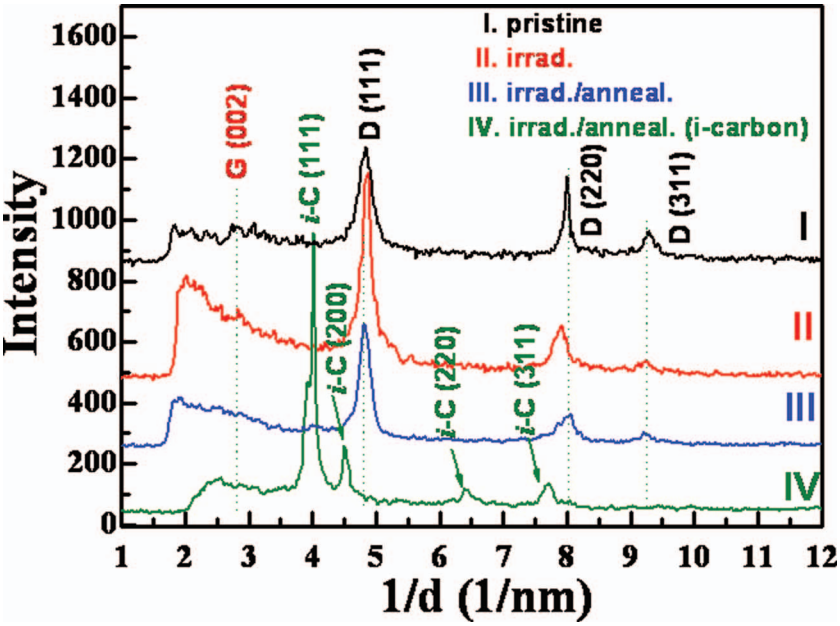

FIG. 14. The linear diffraction patterns (*ldp*) derived from the SAED shown in Fig. 11, corresponding to (I) pristine, (II) Au-ion irradiated and (III, IV) irradiated/ post-annealed UNCD films.

grain boundary phases into nano-graphite. The dissociation of hydrocarbons produced highly active carbon, which was able to attach to the nano-sized diamond grains, inducing their coalescence into large diamond aggregates. In the meantime, homogeneous nucleation of graphite clusters occurred. Restated, the Ostwald-ripening and homogeneous nucleation processes are readily triggered by the Au-ion irradiation process in UNCD films but not in MCD films. The post-annealing process converts the nano-graphites and possibly the heavily damaged nano-diamond into *i-carbon* particulates. Such a phase evolution process would account for the markedly different behavior in the modification of the EFE properties due to the Au-ion irradiation and post-annealing process for the MCD and UNCD films.

IV. CONCLUSION

The effect of 2.245 GeV Au-ion irradiation with a fluence of approximately 8.4×10^{13} ions/cm^2 and post-annealing processes on the microstructure and electron field emission (EFE) properties of MCD and UNCD films was investigated. For the MCD films, the Au-ion irradiation almost completely suppressed the EFE properties of the MCD films. Post-annealing the Au-ion irradiated films at 1000°C for 1 hour effectively restored the EFE properties of the films. TEM examination revealed that Au-ion irradiation had disintegrated some of the diamond grains, resulting in nano-sized diamond particulates embedded in an amorphous matrix. The post-annealing process recrystallized the diamond grains and converted the amorphous carbon into nano-sized crystalline graphite. It is believed that the phase transformation along the grain boundaries is the main cause of the alteration of the EFE behavior of the MCD films. In contrast, for the UNCD films, the Au-ion irradiation induced a large improvement in the EFE properties, and post-annealing the Au-ion irradiated films at 1000 °C for 1 h slightly degraded the EFE properties of the films. The resulting EFE behavior was still markedly better than that of pristine UNCD films. TEM examination revealed that the improvement of the EFE properties of the UNCD films was caused by the formation of nanographite along the trajectory of the irradiating ions. The nanographite formed an interconnected path for electron transport that facilitated the EFE process. The induction of the grain growth process by Au-ion irradiation in UNCD films is presumed to insignificantly alter the EFE properties of the films as the aggregates are sparsely distributed and do not block the electron conducting path.

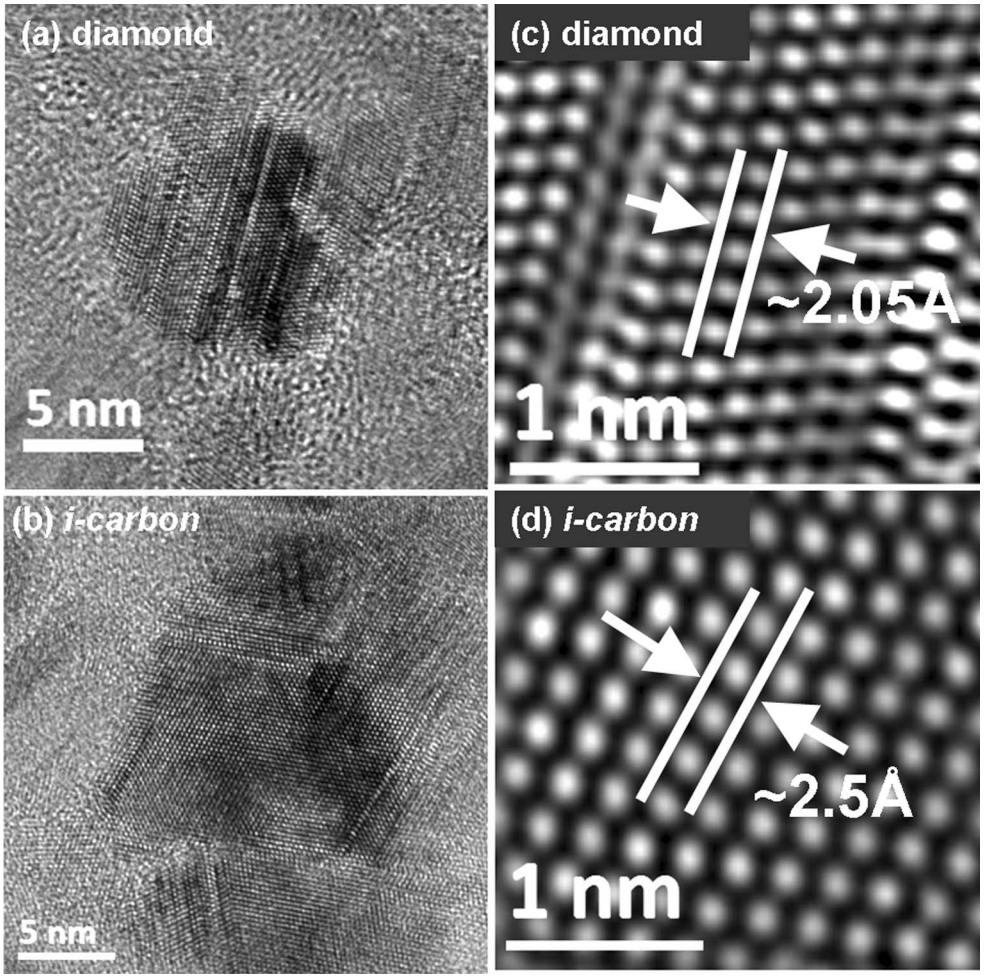

FIG. 15. The TEM structure image of typical small cluster region in Au-ion irradiated/post-annealed UNCD films that contain (a) 3C diamond and (b) *i-carbon* particulates, respectively; (c) and (d) are the enlarged images corresponding to "a" and "b", respectively.

ACKNOWLEDGMENTS

Financial support by the National Science Council, Republic of China, through project No. NSC99-2119-M-032-003-MY2 is gratefully acknowledged by the authors. We acknowledge Dr. Christina Trautmann and the Materials Research Group of GSI, Darmstadt for their support during GeV irradiation at the XO beamline of the UNILAC.

[1] F. J. Himpsel, J. A. Knapp, J. A. VanVecten, and D. E. Eastman, Phys. Rev. B **20**, 624 (1979).
[2] W. Zhu, G. P. Kochanski and S. Jin, Science **282**,1471 (1998).
[3] B. Dischler, C. Wild, W. M-Sebert, and P. Koidl, Physica B **185**, 217 (1993).
[4] T. D. Corrigan, D. M. Gruen, A. R. Krauss, P. Zapol, R. P.H. Chang, Diam. and Relat. Mater. **11**, 43 (2002).
[5] J. Birrell, J. A. Carlisle, O. Auciello, D. M. Gruen and J. M. Gibson, J. Appl. Phys. **81**, 2235 (2002).
[6] E. Rohrer, C. F.O. Graeff, R. Janssen, C. E. Nebel, H. Guettler and R. Zachai, Phys. Rev.B **54**, 7874 (1996).
[7] D. Zhou, A. R. Krauss, L. C. Qin, T. G. McCauley, D. M. Gruen, T. D. Corrigan, R. P.H. Chang, H. Gnaser, J. Appl. Phys. **82**, 4546 (1997).
[8] R. Kalish, Carbon **37**, 781 (1999).
[9] S. Talapatra, J. Y. Cheng, N. Chakrapani, S. Trasobares, A. Cao, R. Vajtai, M. B. Huang, P. M. Ajayan, Nanotechnology **17**, 305 (2006).
[10] S. Prawer, R. Kalish, Phys. Rev. B **51**, 15711 (1995).
[11] K. Panda B. Sundaravel, B. K. Panigrahi, P. Magudapathy, D. N. Krishna, K. G.M. Nair, H. C. Chen, I. N. Lin; J. Apply. Phys. **110**(4) 122115 (2011).

[12] E. J. Correa, Y. Wu, J. G. Wen, R. Chandrasekharan and M. A. Shannon, J. Appl. Phys. **102**, 113706 (2007).
[13] J. Krauser, J.-H, Zollondz, A. Weidinger, C. Trautmann, J. Appl. Phys. **94**, 1959 (2003).
[14] N. Koenigsfeld, H. Hofsass, D. Schwen, A. Weidinger, C. Trautmann and R. Kalish, Diam. and Relat. Mater. **12**, 469 (2003).
[15] S. Prawer, A. Hoffman, R. Kalish, Appl. Phys. Lett. **57**, 2187 (1990).
[16] W. Zhu, G. P. Kochanski, S. Jin, L. Seibles, D. C. Jacobson, M. McCormac and A. E. White, Appl. Phys. Lett. **67**, 1157 (1995).
[17] N. Dilawar, R. Kapil, V. D. Vankar, D. K. Avasthi, D. Kabiraj, G. K. Mehta, Thin Solid Films **305**, 88 (1997).
[18] A. Dunlop, G. Jaskierowicz, P. M. Ossi and Della-Negra, Phys. Rev. B **76**, 155403 (2007).
[19] P. T. Pandey, G. L. Sharma, D. K. Avasthi, V. D. Vankar, Vacuum **72**, 297(2004).
[20] P. M. Koinkar, R. S. Khairnar, S. A. Khan, R. P. Gupta, D. K. Avasthi and M. A. More, Nucl. Instr. and Meth. **B244**, 217 (2006).
[21] J. F. Ziegler, J. P. Biersack, and U. Littmark, *The Stopping and Ranges of Ions in Solids*, Pergamon, New York, 1985.
[22] R. H. Fowler, L. Nordheim, Proc. R. Soc. A **119**, 173 (1928).
[23] I. N. Lin, H. C. Chen, C. S. Wang, Y. R. Lee, and C. Y. Lee; Nanocrystalline diamond microstructures from Ar/H_2/CH_4-plasma chemical vapour deposition, CrystEngComm in press (2011).
[24] Z. Sun, J. R. Shi, B. K. Tay, S. P. Lau; Diam. and Relat. Mater. **9**, 1979 (2000).
[25] A. C. Ferrari and J. Robertson; Phys. Rev. B **63**, 121405 (2001).
[26] J. Michler, Y. Von Kaenel, J. Stiegler, and E Blank; J. Appl. Phys. **81**(1) 187 (1998).
[27] A. C. Ferrari and J. Robertson; Phys. Rev. B **61**, 14095 (2000).